Steel and Composite Structures, *Vol. 22, No. 3 (2016) 537-565*
DOI: http://dx.doi.org/10.12989/scs.2016.22.3.537

Design and modelling of pre-cast steel-concrete composites for resilient railway track slabs

Olivia Mirza [1a], Sakdirat Kaewunruen [*2], Kenny Kwok [1b] and Dane W.P. Griffin [3c]

[1] *School of Computing, Engineering & Mathematics, University of Western Sydney, Kingswood, NSW 2747 Australia*
[2] *Birmingham Centre for Railway Research and Education, School of Engineering, The University of Birmingham, Edgbaston, B15 2TT, UK*
[3] *Rondo Consulting Pty Ltd., Penrith, NSW 2750 Australia*

(*Received October 11, 2015, Revised October 18, 2016, Accepted October 18, 2016*)

Abstract. Australian railway networks possess a large amount of aging timber components and need to replace them in excess of 280 thousands m^3 per year. The relatively high turnover of timber sleepers (crossties in a plain track), bearers (skeleton ties in a turnout), and transoms (bridge cross beams) is responsible for producing greenhouse gas emissions 6 times greater than an equivalent reinforced concrete counterparts. This paper presents an innovative solution for the replacement of aging timber transoms installed on existing railway bridges along with the incorporation of a continuous walkway platform, which is proven to provide environmental, safety and financial benefits. Recent developments for alternative composite materials to replace timber components in railway infrastructure construction and maintenance demonstrate some compatibility issues with track stiffness as well as structural and geometrical track systems. Structural concrete are generally used for new railway bridges where the comparatively thicker and heavier fixed slab track systems can be accommodated. This study firstly demonstrates a novel and resilient alterative by incorporating steel-concrete composite slab theory and combines the capabilities of being precast and modulated, in order to reduce the depth, weight and required installation time relative to conventional concrete direct-fixation track slab systems. Clear benefits of the new steel-concrete composites are the maintainability and constructability, especially for existing railway bridges (or brown fields). Critical considerations in the design and finite element modelling for performance benchmarking of composite structures and their failure modes are highlighted in this paper, altogether with risks, compatibilities and compliances.

Keywords: railway infrastructure; resilient track slabs; modular components; precast composites; construction; maintenance; replacement; bridge

1. Introduction

All components of a railway track system are designed to work together in order to transfer the

*Corresponding author, Senior Lecturer in Railway and Civil Engineering (Ph.D., CPEng.); Visiting BRIDGE Professor in Sustainability & Nanomechanics Laboratory in University of Illionois at Urbana, E-mail: s.kaewunruen@bham.ac.uk
[a] Ph.D., Senior Lecturer in Civil Engineering, E-mail: o.mirza@uws.edu.au
[b] Ph.D., Professor of Structural Dynamics and Wind Engineering, E-mail: k.kwok@uws.edu.au
[c] M.Eng., Structural Engineer, E-mail: dane.griffin@rondo.com.au

 ISSN: 1229-9367 (Print), 1598-6233 (Online)

imposed dynamic loads from the wheels of the railway vehicle to the foundation or support structure of the track (Remennikov and Kaewunruen 2008, 2014, Remennikov *et al*. 2012). These dynamic loads include both vertical loads influenced by the unsprung mass of the vehicles and lateral loads mobilized by centrifugal action of cornering or the momentum of breaking vehicles (Griffin *et al*. 2014, 2015). In general, two dominant forms of railway structures are ballasted and non-ballasted tracks. Bonnett (2005) defined 'ballasted tracks' as incorporating an intermediate layer known as the 'trackbed' comprising ballast and sub-ballast (or called 'capping layer' in Australia) to effectively distribute the vehicle loads to the compacted soil layer called 'sub-grade' (Indraratna *et al*. 2011). If the intermediate load distribution layer is forgone and the track supporting members bear directly on the sub-grade or the superstructure of a bridge or tunnel it is known as a non-ballasted track system. Based on the current design approach, the design life span of structural concrete components is around 50 years (Standards Australia 2003a). Figs. 1(a)-(b) shows a typical railway infrastructure (i.e., railway transom bridge) with existing physical constraints. The rail track is built on timber cross beams, so-called 'transoms', which are supported by long-span steel girders between bridge piers. Recently, there has been a significant attempt to convert such transom bridges into direct-fixation track slab bridge as shown in Fig. 1(c). The design methodology and procedure for track slabs generally yields heavy concrete slabs with a thickness of over 220 mm. As a result, the vertical levels (or heights) of adjacent systems such as fastening systems, rails, overhead wires, platforms and existing bridge girders must comply with such track slabs (Kaewunruen 2007, 2014, Kaewunruen *et al*. 2014, Li *et al*. 2012, 2014).

(a) Typical elevated transom bridge with vertical space constraints from roof trusses

(b) Aging railway transom bridge

(c) Railway slab track or direct fixation adjacent to existing platforms

Fig. 1 Railway infrastructure

Although concrete structures have been popularly used in railway tracks for a long time, demand to improve serviceability and functionality of rail infrastructure components is still significant. In renewal and replacement of aging railway infrastructure systems and components, physical constraints are often exposed. Some examples are the limitation of bearing capacity of existing bridge steel girders, low platform and track clearances, insufficiency of spaces and cross sections of track structures, and so on. In addition, replacing new components within aging systems requires compatibility, compliance and consistency of strengths, properties and characteristics of those new components (Ferdous *et al*. 2015, Kaewunruen 2013). These specific situations have resulted in recent adoption of new alternative materials in railway construction and maintenance. Taking into account constructability and maintainability, this study presents a novel design of resilient composite structures for railway applications. The iconic Sydney Harbour Bridge was used to demonstrate the innovative design of the composite railway track supports.

2. Railway bridge's track support structures

Bridge transoms or sleepers are the members oriented perpendicular to the rails and distribute the rail vehicle loads imposed through the rail to the ballast or superstructure below. Transoms also provide lateral separation of the rails and stability of gauge width between the rails. Currently the most common materials used for intermediate transoms on railway bridges are hardwood timbers. Feasible alternatives for the replacement of deteriorated hardwood timber transoms have been developed recently in Australia. According to Ferdous *et al*. (2015), existing materials used for railway transoms are timber, concrete and steel with each having their own strengths and weaknesses. Their study disregards both concrete and steel as viable alternatives to timber transoms for the following reasons.

Due to high-frequency dynamic forces, high stiffness characteristics and reduced capacity to flex under load (poor tensile strength), traditional concrete transoms typically require a much deeper section than timber transoms. This depth makes traditional concrete transoms relatively expensive and quite heavy, with a typical weight of 285 kg. It was also found that concrete structures tend to be the most cost-effective solution for the railway sleeper application in plain tracks. Benefit cost ratio of concrete sleepers was superior to composites (Kaewunruen and Remennikov 2007, 2009a, b). In contrast, concrete transoms for railway bridge application fail to enter the rail market due to excessive weight and thickness. For railway bridges, design of track support components (e.g., transoms) is generally governed by vertical space. Many railway bridges have been converted to provide track support with concrete slabs. The precast concrete slabs are often heavy (requiring larger supporting bridge structures), but they are much thinner compared with concrete transoms. However, in many practical cases, such conversion is not always possible due to aging bridge structural systems and associated foundation (Remennikov *et al*. 2011, Atmaca and Ates 2012, Pecce *et al*. 2012, Domingo *et al*. 2014).

Recent developments of new materials and composites are aimed at meeting this opportunity. Fibre composite transoms have been installed on a railway bridge in a coal network in Hunter Valley, NSW Australia. Field reports suggested that there were some technical issues associated with failed fixture bolts and helical spring washers used to pin the fibre composite down to steel girders (Kaewunruen 2013, Ferdous *et al*. 2015). The fastening system with significant vibration suppression characteristics has become a new area of research and development in a way that it could aid concrete and composite track supporting structures to withstand dynamic loading

conditions. According to Shanmuganathan *et al*. (2011), fibre composite transoms would not be a feasible alternative as the relatively new technology would require "intensive pre-testing prior to installation on the bridge" and would not be cost effective. Manalo *et al*. (2010) did not considered the use of composite concrete and steel as a replacement alternative to timber transoms. Likewise, none of the intermediate transom material replacement alternatives above address the issue of continuity of the walkway services platform on the railway bridge and these options will be evaluated in this study (Griffin *et al*. 2014, 2015, Kirkland and Uy 2015).

3. Sydney Harbour Bridge (SHB)

The Sydney Harbour Bridge (SHB) was designed by "Dr John Job Crew Bradfield" and its construction was undertaken and completed in 1932 by British firm Dorman Long and Co. It consists of 10 approach spans, 5 on the northern and 5 on the southern approaches to the 503 m long main span, which was achieved by a riveted steel through arch incorporating a suspended steel/concrete deck as shown in Fig. 2(a). The main span crosses Sydney Harbour from Daws point to Milsons point. The bridge originally consisted of two rail tracks, six vehicle lanes and two tramways side by side. The tramways have since been replaced by two more vehicle lanes resulting in the current bridge configuration shown in Fig. 2(b) consisting of a cycleway, two rail tracks, eight vehicle lanes and a walkway. The system carries two of the main railway lines used for passenger and light freight in Sydney, the up and down North shore lines. The Up line refers to the line running toward Sydney's central business district (CBD) and the Down line refers to the line running away from Sydney's CBD. The two railway lines are located on the western edge of the bridge and consist of intermediate timber transoms supported by the steel stringers of the bridge. Fig. 2(c) provides a representation of the current rail configuration over the main span of the SHB. The railway corridor is almost 12000 mm wide and the stringers are spaced at approximately 2000 mm centres, furthermore, the transoms cantilever over the stringer supports by approximately 1200 mm.

The main disadvantage of timber transoms is its susceptibility to degradation, the current transoms used on the SHB have an average life span of between 15 and 20 years depending on the loading condition. This relatively short life span leads to a higher demand for timber transoms which has a flow on effect regarding maintenance cost, supply and quality (Shanmuganathan *et al*. 2011). Another disadvantage of timber is its susceptibility to fire and this is one reason why track grinding is not permitted on the SHB. Track grinding removed the imperfections from the rails which in turn reduce the dynamic impact loads associated with poor wheel to track interaction. Track imperfections can dramatically increase the dynamic loads and therefore reduce the service life of the system. According to a recent critical literature review (Griffin *et al*. 2014), the magnitude of a dynamic load excited by track imperfections can be as high as 600 kN, contrasting this to a typical static axial load which could be as little as 110 kN. The current timber transoms are spaced at 550 mm centres and they do not provide a continuous and impervious platform across the stringers and girders of the bridge. Aside from the timber deck between the lines and the guard rails between the tracks, the area directly below and approximately 500 mm to either side of each rail is uncovered with the exception of the transoms themselves. This uncovered area is a cause for concern as it allows for water egress to the stringer top flanges which is not desirable with regards to corrosion and also poses the problem of foreign objects falling from the railway corridor to parks, roads and waterways beneath the bridge.

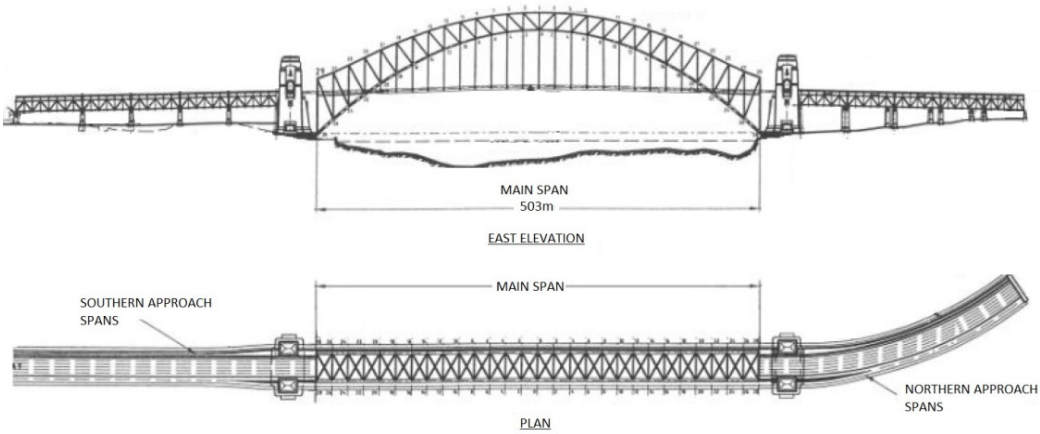

(a) Elevation and plan view

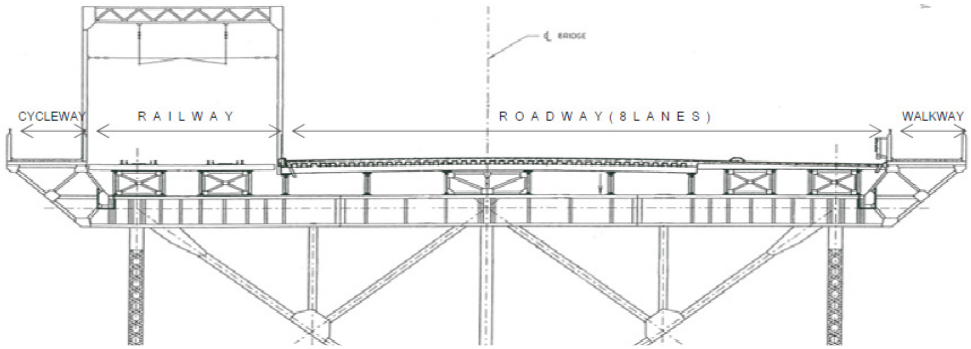

(b) Cross section showing the current configuration

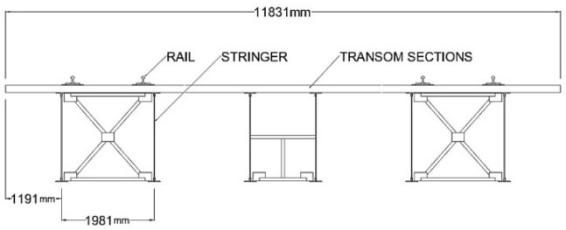

(c) Cross section showing the current configuration of the rail corridor of the SHB

Fig. 2 Sydney Harbour Bridge

4. Design of composite track slabs

4.1 Design fundamental

This study has been initiated through consultation with industry partners RailCorp with the specific objective of determining the feasibility of and providing design solutions for composite concrete and steel "panels" to replace the existing timber transoms within the rail corridor on the main span of the Sydney Harbour Bridge. Steel rails and guard rails will be installed using special

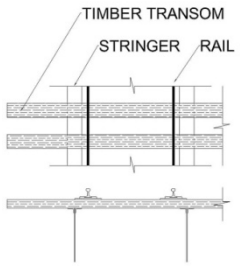

(a) Plan and part section

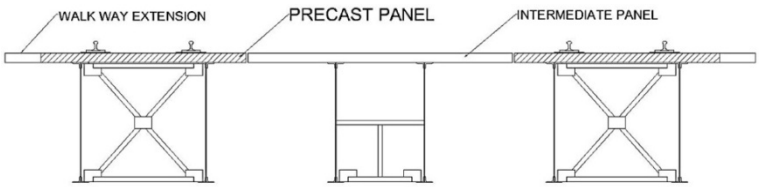

(b) Proposed break-up current transons

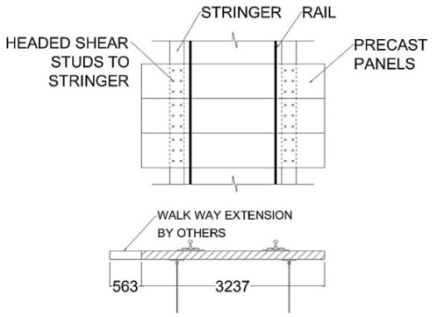

(c) Plan and section of proposed precast panel configuration

Fig. 3 Sydney Harbour Bridge

baseplates and rail pads onto these composite panels. The replacement transom alternatives shall provide a solid rail corridor similar to that of slab track. Although unlike slab tracks, the research herein has focused on using composite theory enabling the depth and hence, the weight of the replacement panels to be less than that of typical slab track systems. This solid and continuous surface will alleviate the need for the timber decking boards between the railways, prevent water egress to the girder top flanges and arrest foreign objects from falling to the habitable areas below the bridge. Installation time is required to be minimized to lessen the impact of excessive rail possession. This will be achieved by designing the panels as precast, so they can be transported to site and installed relatively quickly.

Fig. 3(a) illustrates an idealized plan view of the current intermediate timber transom track configuration with the intermediate timber transoms spaced at 550 mm centres spanning between the stringers and providing support to the rails. While Figs. 3(b) and (c) show the proposed configuration with the precast composite panels also spanning between the stringers and supporting the rails while providing a continuous rail platform. The panel designs presented herein have disregarded the 563 mm outstand shown in Fig. 3(b) as being ancillary to the design. To assist in retrofitting the precast panels to the existing stringer flanges, the panels shall be cast with holes at the headed shear stud locations indicated in Fig. 3(c). It is anticipated that the panels will be placed over the bridge stringers, the shear stud connecters will then be installed and the holes filled with non-shrink grout to secure the panels in place. The application of blind bolts as shear connectors can be adopted for conventional shear stud connectors (Griffin *et al*. 2014, 2015).

The panel design solutions shall ensure no increase in rail level occurs upon replacement of timber transoms. This is achieved by limiting the maximum depth of the panels beneath the rail pads to 180 mm, which is in line with the depth of the current timber transoms. Maintaining the

Table 1 Load combinations for SHB panel (developed as per Figure 3)

Limit states	Action	Load Combination (LC)	Application
Ultimate	Moment	LC1 = 1.4 G_{panel} + 3.25 Q_{300LA} + 1.6 $Q_{breaking}$	Panel UDL + Pad UDL
	Shear and reactions	LC2 = 1.4 G_{panel} + 2.70 Q_{300LA} + 1.6 $Q_{breaking}$	Panel UDL + Pad UDL
	All	LC3 = 1.4 G_{panel} + 1.5 $Q_{General}$	Panel UDL
	All	LC4 = 1.4 G_{panel} + 1.6 Q_{nosing}	Panel UDL + Longitudinal point
	All	LC5 = 1.4 G_{panel} + 1.2 Q_{derail}	Panel UDL + Point
	All	LC6 = 1.4 G_{panel} + 1.0 W_{vu*}	Panel UDL
	All	LC7 = G_{panel} + Q_{300LA} + $Q_{breaking}$ + W_{vu*}	Panel UDL + Pad UDL
Serviceability	Deflection	LC10 = 1.2 G_{panel} + 2.03 Q_{300LA} + 0.7 W_{vs*}	Panel UDL + Pad UDL

rail level will negate the need to adjust overhead systems and result in cost minimisation. Previous research into the application of composite steel and concrete panels over steel girder bridges conducted by Choi *et al*. (2010) has not considered the application of vehicle derailment loads. The application of precast panels over the SHB herein requires a portion of the panels to cantilever over the supports. The application of derailment loads applied to these cantilevered ends induces considerable negative bending moments and shear forces over the support. It is necessary for this study to provide a design and analysis for two variations of precast panels, one to accommodate derailment loads, which will be referred to as "*Derailment panels*"; and the other to accommodate standard in-service loads, which will be referred to as "*In-service panels*".

4.2 Design Load Combination (LC)

In principle, Rail Authority (RailCorp 2010, 2013a, b) outlines the minimum design criteria for new and existing underbridges and suggested loads applicable to railway components such as live and derailment loads be adopted as specified within Australian Standard AS5100.2 (2004). Design loads and load combinations specified within AS5100.2 (2004) are applicable for consideration in the design of the composite steel and precast concrete panels. The load combinations adopted from AS5100 (2004) clause 22 can be tabulated as a case study in Table 1.

4.3 Structural materials

4.3.1 Concrete

The concrete characteristic compressive cylinder strength after 28 days of curing (referred to as f'_c) has been adopted as 50 MPa for durability. The exposure classification for the design of the SHB is considered for surface and exposure environment in "Coastal and any climatic zone". Australian Standard AS3600 (2009) suggests a minimum concrete strength f'_c of 40 MPa. On this ground, two parameters can be modified in order to obtain the shallowest member profile possible, these are to increase the compressive strength of the concrete and to maximize the moment arm between the internal compressive and tensile forces (then reducing the load action). The latter is achieved by moving the conventional top reinforcement for hogging strength as close to the surface of the members as possible, which reduces the cover over the reinforcing steel. A

minimum concrete cover over the conventional reinforcement of 35 mm is recommended when using concrete with a $f'_c \geq 50$ MPa (Standards Australia, 2009). Note that the necessity to minimize cover and maximize f'_c has led to the adoption of $f'_c = 50$ MPa as stated above. Increasing f'_c may yield greater flexural capacities however; f'_c must not be less than 40 MPa due to durability concerns.

4.3.2 Tensile and shear reinforcement

According to Australian Standard AS / NZS 4671:2001 (Standards Australia 2003), steel reinforcing material of D500N grade has been adopted for all conventional reinforcing steel. The 'D' stands for deformed, 'N' stands for normal ductility and the 500 stands for 500 MPa, which is the yield stress of the reinforcement.

4.3.3 Profiled steel sheeting

The profiled steel sheeting adopted for design is the Bondek II profile, manufactured by BHP Building Products and has been selected for a number of reasons. The Bondek II section, commercially available, is manufactured from high tensile steel with a yield strength of 550 MPa. It has a zinc coating for corrosion protection and durability and is available in 0.60 mm, 0.75 mm and 1.00 mm base metal thickness (Goh *et al*. 1998). 1.00 mm BMT will be adopted for the design. The standard module width for Bondek II is 600 mm with three troughs of approximately 180 mm in width which makes the profile suitable to accommodate three equally spaced sets of shear stud fixings to the bridge stringer. Handling and installation manageability along with manufacturing and installation time have been considered in the selection of the panel width. While it may be easier the handle narrower panels, it is desirable to maximize the panel width to reduce the number required to be manufactured and installed. The 600 mm panel width has been selected as an appropriate medium between the two criteria.

It is common practice to install fastening systems at 500 mm interval over track support structures as the reduction in spacing reduces the reaction at each rail pad. However, to ensure symmetry of the design and analysis herein, the fastening systems have been designed to be spaced at 600 mm centres.

4.4 Flexural capacity design

The negative moment regions of the panels have been designed as singly reinforced beams as per AS3600 (2009) with standard top reinforcement in tension and no contribution of the profiled steel sheeting in compression. The panels have been designed as under reinforced members by assuming tensile reinforcement has yielded to avoid brittle collapse at ultimate loading, this assumption is verified by calculations (Griffin *et al*. 2015).

The design procedure for determining the positive flexural strength of the precast panels has been adopted from Goh *et al*. (1998) and it incorporates the contribution of the profiled steel sheeting acting compositely with the concrete. Crucial design parameters of the profiled steel sheeting include ultimate yield strength, cross sectional area second moment of area and parameters relating to horizontal shear strength. The design approach adopts simple plastic rectangular stress block theory as shown in Fig. 4. Full scale testing presented by Goh *et al*. (1998) was conducted to determine the mechanical resistance or "rib shear strength" between the Bondek and the concrete in a similar manner to the '$m - k$' method. This rib shear strength, which is nominated as '*Hr'*, is used to determine the degree of shear interaction and in turn the tensile stress

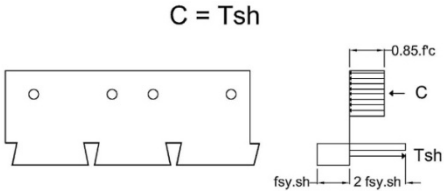

Fig. 4 Plastic rectangular stress block theory (Note that $f_{sy.sh}$ is the yield stress of steel sheets and C is the compression from concrete stress block)

T_{sh} within the sheeting at various distances from the supports. With T_{sh} known, the positive flexural capacity can be obtained.

4.5 Shear capacity design

The design of composite slabs with regards to the vertical shear capacity of both positive and negative bending regions can be significantly affected by the reduction of concrete area due to the dimensions of the profiled steel sheeting ribs. The design principle requires that the area of the concrete removed by the profiled steel sheeting ribs be not greater than 20 per cent of the total slab cross sectional area (Griffin *et al*. 2014). The negative shear capacity of the panels has been calculated in accordance with Australian Standard AS3600 (2009) assuming similarity to a typical reinforced concrete beam incorporating conventional tensile reinforcement and disregarding any contribution from the steel sheet composite action. For the design herein, the positive shear actions consistently occur within the middle span of the panels meaning the profiled steel sheeting is anchored either side of the shear failure plane at the shear stud welding points of each support (Oehlers and Bradford 1995, 1999, Fanaie *et al*. 2015, Lezgy-Nazargah and Kafi 2015). The positive shear capacity of the panels has therefore been calculated in accordance with AS3600 (2009) assuming similarity to a typical reinforced concrete beam with the profiled steel sheeting acting as conventional tensile reinforcement at the full depth of the composite slab.

4.6 Load resistance design

The following design calculations are for the bending moment capacities to support the negative bending moments (-*ve*)*M**1 and (-*ve*)*M**2 in the precast 'derailment' panels due to derailment loading conditions as shown in Fig. 5(a). Similarly, when neglecting the tensile capacity of concrete, the positive bending moment in the precast 'in-service' panels could be designed in the same way as that of a beam.

Step 1: Check yielding of the reinforcement

$$k_u = A_{st} f_{sy} / \alpha_2 f'_c . \gamma . d . b \tag{1}$$

Step 2: Check bending moment capacity

$$\begin{aligned} \phi M_u &= \phi \times T \times z \\ \phi M_u &\geq {}_{(-ve)} M^* 1 \end{aligned} \tag{2}$$

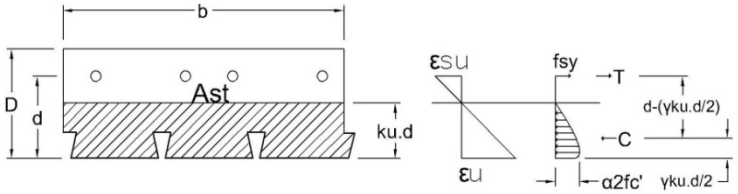

(a) design diagram for negative bending moment (*-ve*)*M**

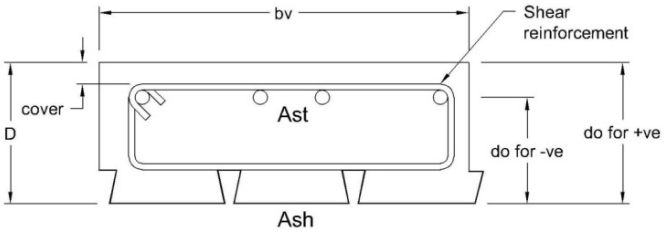

(b) design diagram for shear (-ve)V*

Fig. 5 Derailment resistance design

Step 3: Check minimum reinforcement

$$A_{st.\min} = \alpha_b.(D/d)^2.(f_{ct.f}/f_{sy})b.d$$
$$A_{st} \geq A_{st.\min} \tag{3}$$

The following design calculations are for the positive and negative shear capacities to support the shear action (*-ve*)*V** in the precast panels due to in-service and derailment loading conditions as shown in Fig. 5(b).

Step 1: Check web crushing

$$\phi V_{u.\max} = \phi 0.2 f_c' b_v d_o \tag{4}$$

Step 2: Check shear strength of concrete

$$V_{uc} = \beta_1\beta_2\beta_3 b_v d_0 f_{cv}\left(\frac{A_{st}}{b_v d_0}\right)^{\frac{1}{3}} \tag{5}$$

Step 3: Check minimum reinforcement

$$V_{u.\min} = V_{uc} + 0.1\sqrt{f_c'}b_v d_0 \geq V_{uc} + 0.6 b_v d_0 \tag{6}$$

Step 4: Check minimum shear reinforcement

$$\frac{A_{sv,\min}}{s} \geq \frac{0.06\sqrt{f_c'}b_v}{f_{sy,f}} \geq \frac{0.35 b_v}{f_{sy,f}} \tag{7}$$

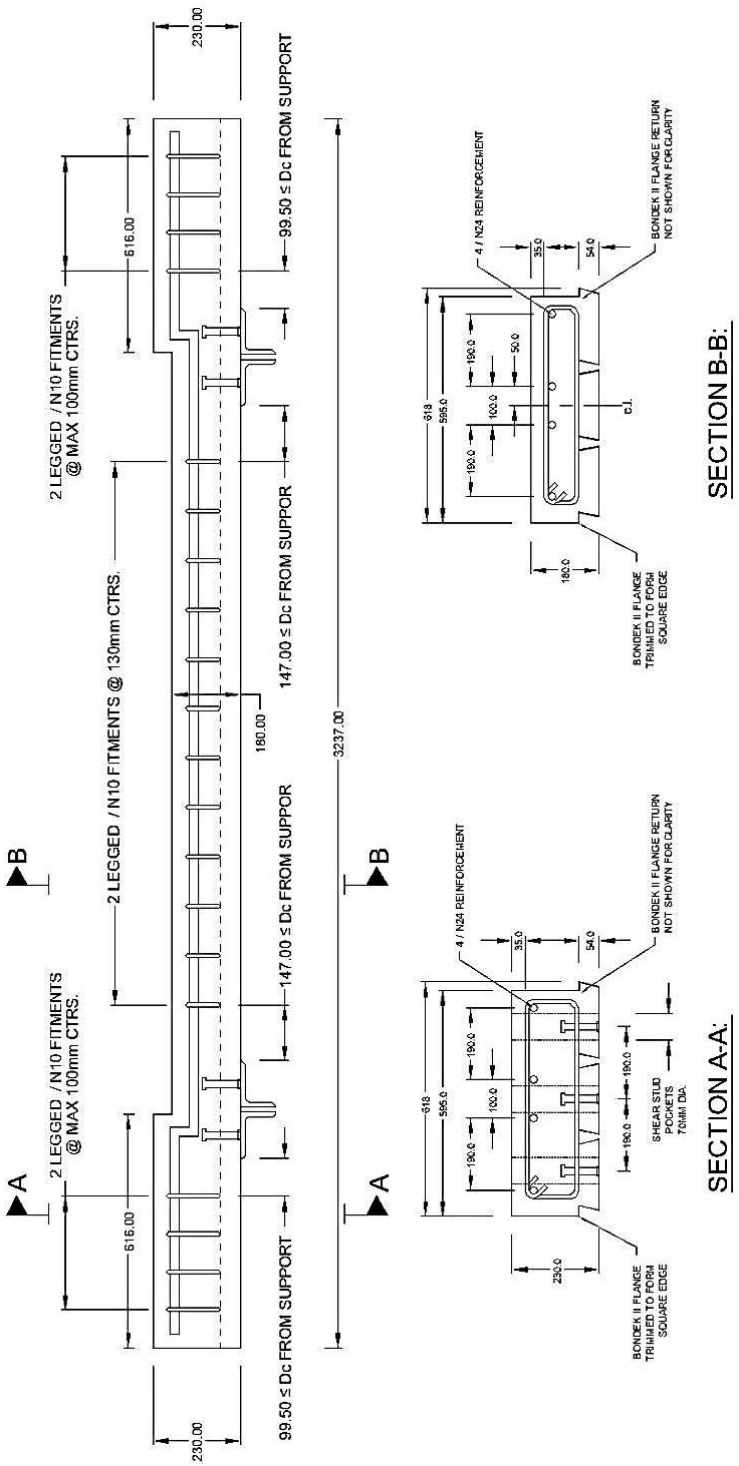

(a) Derailment composite panel

Fig. 6 Precast composite panels for track support structure

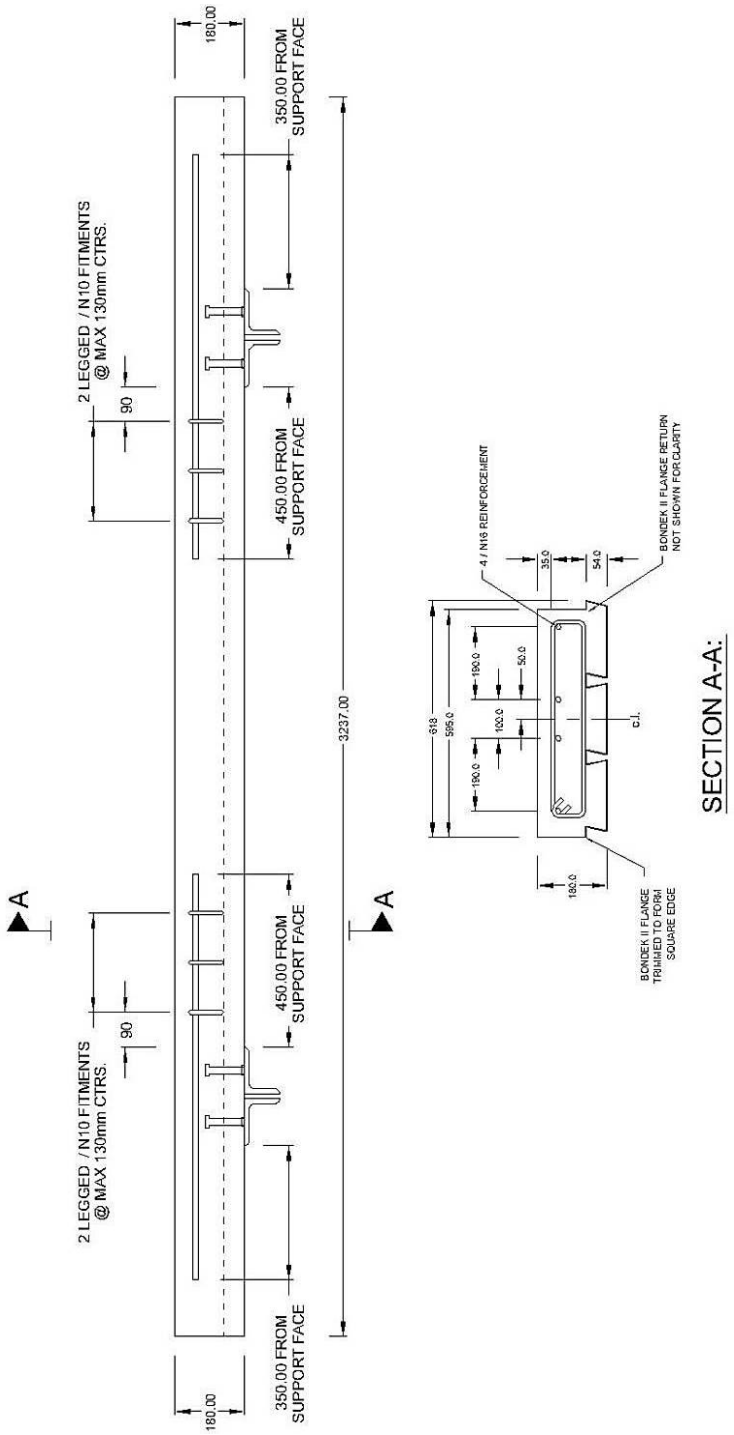

(b) In-service composite panel

Fig. 6 Continued

4.6 Design of composite panels

Fig. 6 exhibits the design outcome of steel-concrete composite panel for the track support structure. Derailment panels are required to be 180 mm thick for the mid-span of the panels and below the fastener locations. The depth of the panel within 616 mm from the edge is required to be increased to 230 mm to accommodate the substantial negative bending moments induced by the derailment loads. The panels require 4 off N24 reinforcement bars throughout the length and 2 legged N10 shear fitments are also required throughout the length as shown. This is due to the fact that derailment loads could be applied at any location within the panel (Griffin *et al*. 2014).

Table 2 provides a summary of the design actions imparted on the panels as well as the corresponding design capacities of the panel detailed within Fig. 6 to resist each design action. Fig. 6a shows the design outcome for derailment panel and Fig. 6(b) shows that of the in-service panel (excluding the derailment load). The design ratio shown in Table 2 equals the design capacity divided by the design action and must be greater than 1 for the design to be sufficient. It can be noted here that the 180 mm depth of the-mid span is controlled by the shear capacity of the derailment panels while the edge depth is controlled by the negative flexural strength of the panel. Further research into the resistance of shear actions by the precast composite concrete and steel panels may be effective in yielding a reduction in mid span panel depth (Griffin *et al*. 2015).

5. Modelling

5.1 Materials

A three dimensional finite element of model of the steel-composite track support panel has been developed using a finite element package ABAQUS. The model has been validated using previous work by Mirza *et al*. (2010, 2011). In this model, concrete has been modeled using elasto-plastic elements in ABAQUS. Plain concrete with the design compressive strength (f'_c) of 50 MPa has been adopted for use in the finite element analysis of thepanels. The non-linear behaviour of the plain concrete under ambient conditions is represented in Fig. 7(a), which shows three distinct portions of the stress strain curve. There are two parts to the curve within the compressive section, which makes up the non-linear behaviour of the concrete. ABAQUS requires the Young's modulus of concrete (E_c) and poisons ratio (v) to calculate the first part of the stress strain curve, which is

Table 2 Summary of composite panel design capacities

(a) Summary of Derailment panel design capacity

Design action		Design capacity		Design ratio
(+ve) M^*	46.33 (kNm)	ϕM_{uo}^{+}	62.4 (kNm)	1.34
(-ve) M^*1	-108 (kNm)	$\phi M_{u.1}^{-}$	-112 (kNm)	1.03
(-ve) M^*2	-58 (kNm)	$\phi M_{u.2}^{-}$	-76 (kNm)	1.31
(+ve) V^*	142 (kN)	ϕV_u^{+}	142 (kN) *	1.00
(-ve) V^*	-217 (kN)	ϕV_u^{-}	-217 (kN) *	1.00

* = Design shear capacities are conservative as the fitment spacing has been rationalised in accordance with slab depth. For example, the shear fitment spacing required to achieve the design capacities shown may be greater than the shear fitment spacing nominated due to design standards.

Table 2 Continued

(b) Summary of in-service panel design capacity

Design action		Design capacity		Design ratio
(+ve) M^*	6.30 (kNm)	ϕM_{uo}^{+}	62.94 (kNm)	9.9
(-ve) M^*	-35.41 (kNm)	ϕM_{u}^{-}	-38.31 (kNm)	1.08
(+ve) V^*	94.48 (kN)	ϕV_{u}^{+}	94.48 (kN) *	1.00
(-ve) V^*	-94.48 (kN)	ϕV_{u}^{-}	-94.48 (kN) *	1.00

* = Design shear capacities are conservative as the fitment spacing has been rationalised in accordance with slab depth. For example, the shear fitment spacing required to achieve the design capacities shown may be greater than the shear fitment spacing nominated due to design standards.

assumed to be linear elastic and acts up to a proportional limit stress of 0.4 f'_c (Lam and El-Lobody 2001).

Young's modulus of concrete (E_c) has been calculated to be 34,652 MPa from Eq. (8) adopted from AS3600 (2009) and Poisons ratio (v) of 0.2 has been adopted.

$$(\rho^{1.5}) \times (0.024\sqrt{f_{cmi}} + 0.12) \quad \text{when} \quad f_{cmi} > 40\,\text{MPa} \tag{8}$$

For the second section of the stress strain curve in the compressive region, the stress can be found as a function of strain following Eq. (9) (Mirza *et al*. 2011)

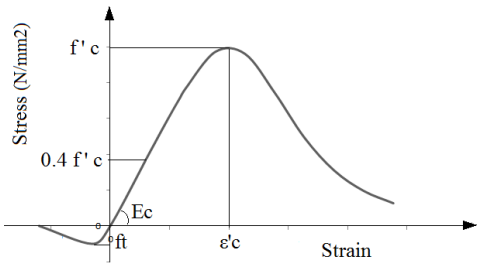

(a) Stress strain curve for normal concrete

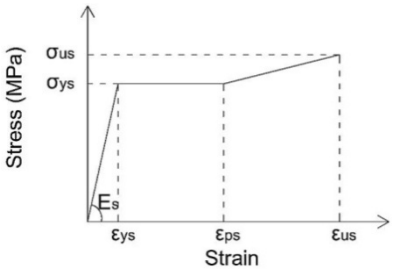

(b) Tri-linear stress / strain curve for stringer and reinforcing steel

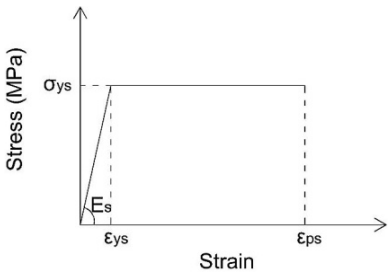

(c) Bi-linear stress / strain curve for profiled steel sheeting and headed shear studs

Fig. 7 Material characteristics for the 3D finite element model

Table 3 Steel element material properties

Element	Yeild stress f_y (MPa)	σ_{us} (MPa)	ε_{ps}	ε_{us}
Stringer	300	1.28 σ_{ys}	10 ε_{ys}	30 ε_{ys}
Reinforcing Steel	500	1.28 σ_{ys}	9 ε_{ys}	40 ε_{ys}
Bondek II	550	N/A	20 ε_{ys}	N/A
Shear Studs	420	N/A	25 ε_{ys}	N/A

$$\sigma_c = \frac{f_c' \gamma \left(\frac{\varepsilon_c}{\varepsilon_c'} \right)}{\gamma - 1 + \left(\frac{\varepsilon_c}{\varepsilon_c'} \right)^{\gamma}} \tag{9}$$

Where

$$\gamma = \left| \frac{f_c'}{32.4} \right|^3 + 1.55 \quad \text{and} \quad \varepsilon_c' = 0.002 \tag{10}$$

In the tension zone the stresses are assumed to increase linearly until the concrete cracks after which the stresses decrease linearly to zero.

Research by Mirza *et al*. (2010) indicated that steel components of a composite system perform differently with regards to stress strain relationships. The study outlined that the stress strain relationship of stringer beams and reinforcing steel can be modelled using a tri-linear curve as shown in Fig. 7(b). These sections are initially linear elastic followed by strain softening and finally yielding. On the other hand, Profiled steel sheeting and headed shear stud connectors were found to be void of strain softening hence the bi-linear curve shown in Fig. 7(c) was used to model the stress strain relationship of these sections. The initial material properties used for modelling the steel elements within ABAQUS are presented in Table 3 with the ratios for determining ultimate stress (σ_{us}), plastic strain (ε_{ps}), and ultimate strain (ε_{us}) being adopted from the extensive research carried out by Mirza *et al*. (2010). Common material properties for steel elements are Young's modulus (E_s) = 200,000 MPa and Poison's ratio (v) = 0.3. Furthermore, the stress strain relationship of the steel is assumed to be similar in both tension and compression.

5.2 Finite element modelling

Solid, three-dimensional, eight node elements incorporating linear approximation of displacements, reduced integration and hourglass control (C3D8R) have been used in this study to model all of the parts with the exception of the steel reinforcing. The C3D8R element type has been found to be sufficient for linear and nonlinear models, and is capable of incorporating contact properties, handling large deformations and accommodating plasticity. The use of C3D8R elements increases the rate of convergence of the solutions (Mirza *et al*. 2010, 2011). C3D8R elements were similarly adopted by Lam and El-Lobody (2001) for modelling the general concrete and steel beams for push tests, however 15 and 20 node elements were adopted for the concrete around the shear studs and the shear studs respectively. The increase of nodes for the elements surrounding the shear stud connection was desirable to more accurately determine load slip

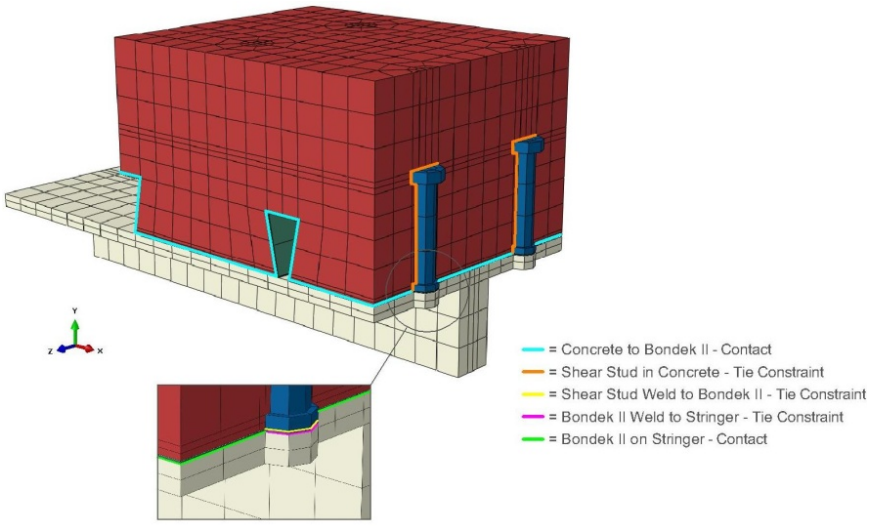

Fig. 8 Part section of panel model - depicting element contacts and constraints

Table 4 Panel deflection sensitivity to mesh size

Mesh set	Part mesh size					Mid span deflection (mm)
	Bondek II	Shear studs	Concrete	Stringer	Steel reinforcing	
1	20	20	20	20	84.7	0.7198
2	30	30	25	25	84.7	0.7329
3	35	30	25	25	84.7	0.7336
4	50	40	40	40	84.7	0.7356
5	60	40	40	40	84.7	0.7323

relationship in these areas. 8 node elements have been determined to provide sufficient accuracy for the models within this study.

Previous research (Mirza and Uy 2009, 2011) adopted S4R elements for modelling the thin walled sections of profiled steel sheeting for composite slabs. These are shell elements of four-nodes with 5 DOF and incorporate reduced integration. Conversely, S4R elements is recommended as being the most suitable for modelling thin walled sections and that S4R elements are more accurate in simulating contact than standard shell elements. As mentioned above, this investigation has adopted solid C3D8R elements for modelling the Bondek II as contact interaction is of considerable importance in this application, furthermore the mesh of the Bondek II has been made relatively small to avoid element aspect ratio issues.

Sensitivity analyses of mesh size and meshing optimization were conducted by Griffin *et al*. (2015) in comparison with previous established model by Mirza and Uy (2009, 2011). Five models were analysed with the mesh size of each part varying for each model. Fig. 8 shows a three-dimensional finite element model of the composite panel for track support structure. Table 4 shows the sensitivity of mesh sizes on the precision of mid-span deflection of bridge-supported composite panel.

Table 5 Master and slave surface designation

Interface	Interface type	Master surface	Slave surface
(a) Reinforcing steel in concrete	Embedded	Reinforcing steel	Concrete
(b) Concrete to Bondek II	Surface to surface contact	Bondek II	Concrete
(c) Shear stud in concrete	Tie constraint	Shear stud	Concrete
(d) Shear stud weld to Bondek II	Tie constraint	Bondek II	Shear stud
(e) Bondek II weld to stringer	Tie constraint	Bondek II	Stringer
(f) Bondek II on stringer	Surface to surface contact	Bondek II	Stringer

5.3 Contact and interface

When defining either interactions or constraints it is necessary to designate a master surface and a slave surface. The surface of the element with the stiffer material is defined as the master surface and the slave surface is assigned to the less stiff element. ABAQUS then places a "kinematic constraint" to ensure that a slave surface cannot penetrate a master surface. The designation of master and slave surfaces based on material stiffness are outlined in Table 5 and catalysed the nomination of the initial mesh sizes provided in Table 4. In this investigation, there are two contact interactions and four tie constraints nominated as A to F. Contact A was used between all reinforcing steel and the concrete and uses the embedded technique. Contact B was between the concrete and Bondek II and employs surface to surface techniques with finite sliding, hard contact in the normal direction and a penalty coefficient of friction of 0.5 in the tangential direction which is in keeping with that adopted in the theoretical designs. Contact F was applied between the Bondek II and the stringer flange and also employs surface to surface techniques with finite sliding, hard contact in the normal direction and a frictionless surface is assumed in the tangential direction.

Previous research suggests contact interactions for the interface between the shear studs and the surrounding concrete with tangential friction coefficients ranging from 0.15 to 0.25 (Mirza and Uy 2009, 2011). This contact interaction was effective for providing accurate results in terms of load slip response of headed shear studs. Studies on composite floor beams concluded that an embedded technique similar to that used for reinforcing steel within concrete is effective for simulating the connection between shear studs and concrete and returns sufficiently accurate results (Nguyen and Kim 2009, Tahmasebinia *et al*. 2012). Tie constraints have been adopted as an intermediate solution between the embedded method and the surface to surface contact method for the connection between the shear studs and the concrete for the models presented in this study. Similarly, tie constraints are used to simulate a mechanically fixed link between two part instances. Tie constraints D and E represent the physical welding of the surfaces of the shear stud contacting the Bondek II and the Bondek II contacting the stringer flange.

5.4 Boundary conditions and load application

The finite element model can be divided into 2 groups: the derailment panel model and the in-service panel model. Only the in-service panel model can be considered symmetrical. The in-service panel model as shown in Fig. 9(a) has been constructed as a half model, symmetrical about the X-axis. Surface 1 in Fig. 9(a) is defined as a symmetrical surface and the nodes of the concrete and Bondek II that lie on this surface have been restricted from translating in the *Z* direction.

Because the response to loading of the stringer is only of secondary importance to the scope of this study, only a portion of it has been modelled as shown in Fig. 9(a). The cut edges of the stringer are labelled as Surface 2 and the nodes of this surface have been restrained from translation and rotation in all three axes, this is defined in ABAQUS as an Encastre boundary condition. The derailment panel model as shown in Fig. 9(b) has been constructed as a full model due to the non-symmetrical loading. Similarly to the in-service half model, the cut edges of the stringers (labelled as Surface 1 in Fig. 9(b)) and the nodes of this surface have been assigned Encastre boundary conditions.

As shown in Table 1, the load combinations LC1 and LC2 produced the worst case design actions resulting from standard in service loads for bending moments and shear forces of the in-service panels respectively. As the FE models are particularly concerned with the flexural response of the precast panels, the loads resulting from LC1 have been adopted for the simulations. The load combination LC5 produced the worst case design actions resulting from derailment loads,

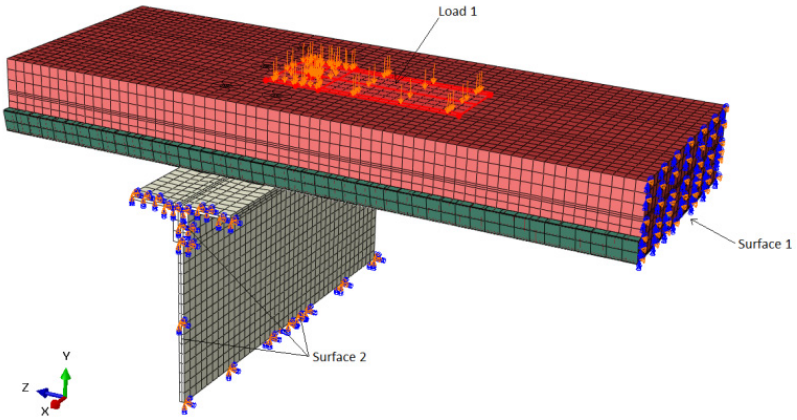

(a) Boundary conditions and loads for the In-service load half model (load transferred from fastening system)

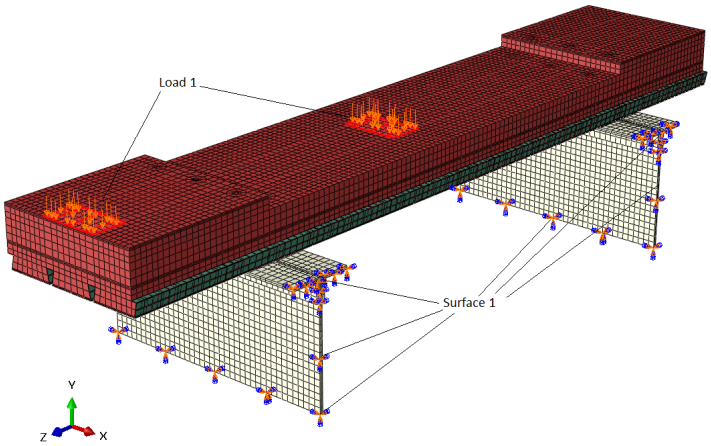

(b) Boundary conditions and loads for the Derailment load model (load from displaced wheels)

Fig. 9 Boundary conditions

therefore the loads resulting from LC5 have been adopted for the simulations of derailment models. The derailment load is assumed to act over the contact area of the wheel and concrete based on the width of the vehicle wheel multiplied by arc length of a 30 degree segment of the wheel. The loads nominated above were applied to each model using the modified RIKS method available within ABAQUS. The RIKS method allows a proportion of the total load to be incrementally applied to the model with the equilibrium iteration check completed for each increment prior to the next proportional load application. Also, mesh optimisation have demonstrated practically suitable numerical results (Bradford and Uy 2007, Griffin *et al*. 2015).

6. Results and discussion

Fig. 6(a) shows the required details for the derailment panels. Derailment panels are required to be 180 mm thick for the mid span of the panels and below the rail pad locations. The depth of the panel within 616 mm from the edge is required to be increased to 230 mm to accommodate the substantial negative bending moments induced by the derailment loads. The panels require 4 off N24 reinforcement bars throughout the length and 2 legged N10 shear fitments are also required throughout the length as shown. This is due to the fact that derailment loads could be applied at any location within the panel. It can be noted here that the 180 mm depth of the mid span is controlled by the shear capacity of the derailment panels while the edge depth is controlled by the negative flexural strength of the panel. Further research into the resistance of shear actions by the precast composite concrete and steel panels may be effective in yielding a reduction in mid span panel depth.

Fig. 6(b) shows the required details for the in-service panels. In-service panels are required to be 180 mm thick throughout their full length. The panels require 4 off N16 tensile reinforcement bars above the support locations as shown. This is due to the negative bending moments induced at the supports due to the assumption of "fixed" connections. 2 legged N10 shear fitments are only required within the critical shear zone near the supports. It can be noted here that the 180 mm depth of the mid span is controlled by the negative flexural strength of the panels to support the negative bending moments induced by the fixed connections and the shear capacity of the panels within the critical zone. However, the panel depth may be further reduced at the cantilevered edges and throughout the middle 850 mm of the panel where shear forces and negative bending moments are no longer present.

6.1 Performance of derailment panel

Deflected shape of the derailment panels subjected to derailment loads is shown in Fig. 10(a). Fig. 10(b) indicates the average stress to derailment load relationship for the critical concrete node and the critical reinforcing steel node, shown in Figs. 10(c) and (d). It can be noted from the load-stress curve that when the surface concrete starts to crack at low stress levels in the tension zone the reinforcing steel starts to sustain the tensile forces. The tensile stresses present within the reinforcing steel at full application of the derailment loads is 56.2 MPa, which is significantly less than the reinforcing steel yield stress of 500 MPa.

Fig. 10(e) indicates the average stress to derailment load relationship for the critical concrete node shown in Fig. 10(f) acting in compression. It can be noted that the stress increases at a constant rate up to a maximum compressive stress of 32.26 MPa at full application of the

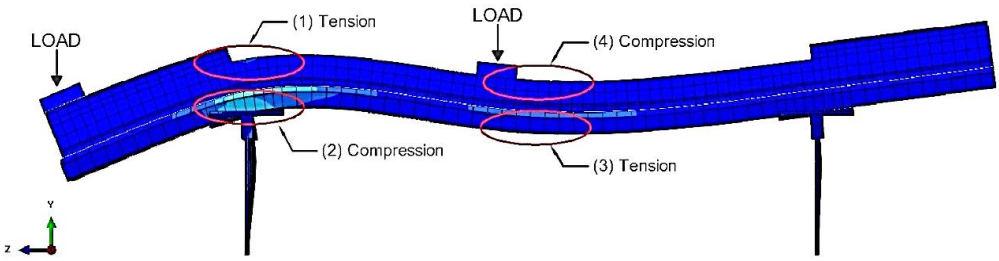

(a) Exaggerated deflected shape of the derailment panel at the full extent of loading

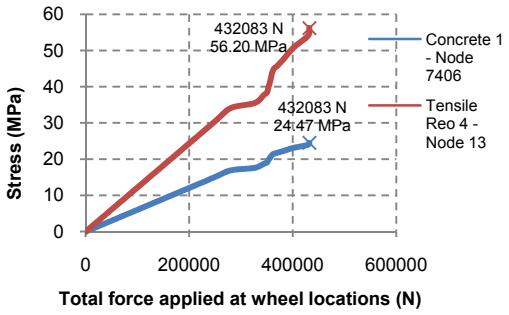

(b) Stress to load relationship for concrete and reinforcing steel nodes within zone (1) Tension

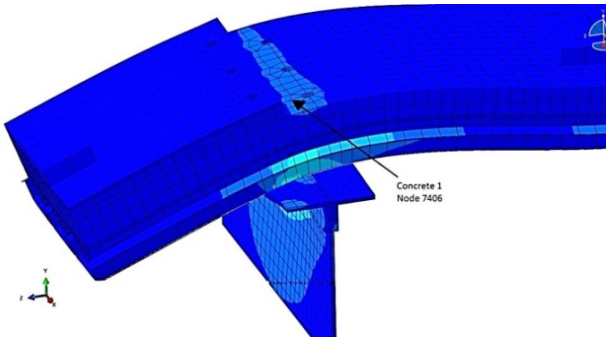

(c) Critical stress concentration zone in Concrete 1 (Node 7406 location)

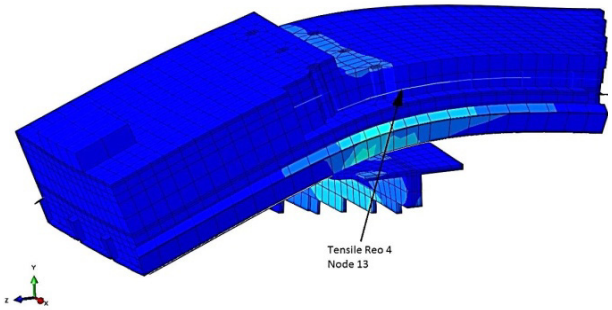

(d) Maximum tensile in reinforcing steel 4 (Node 13 location)

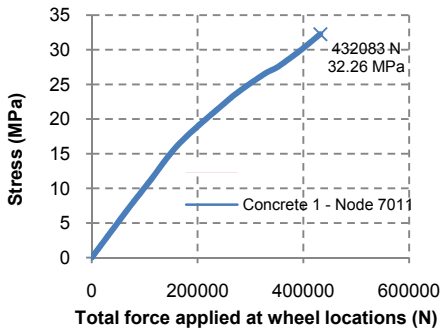

(e) Stress to load relationship for concrete node 7011 within zone (2) Compression

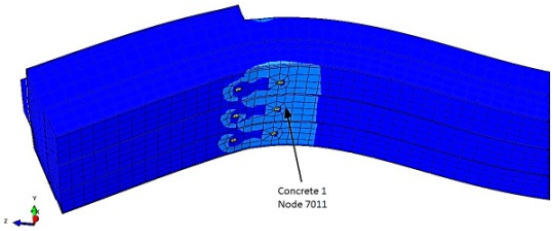

(f) Critical stress at support (Node 7011 location)

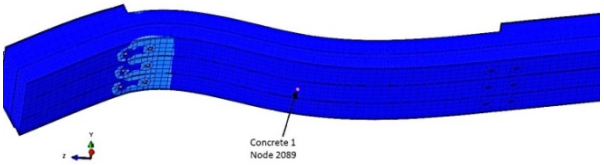

(g) Critical tension of concrete (Node 2089 location)

Fig. 10 Finite element analysis of composite derailment panel – cont

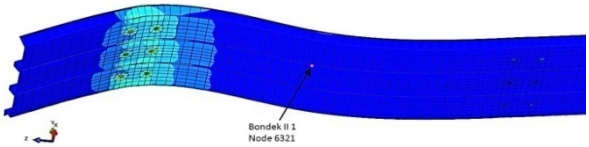

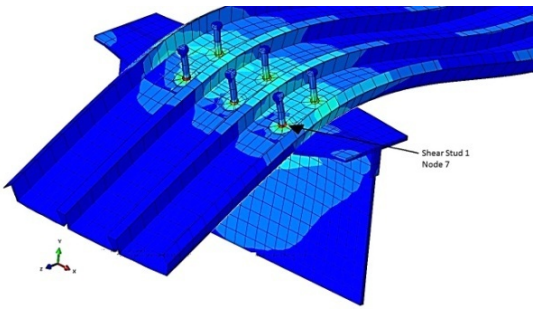

(h) Critical stress of Bondek II 1 (Node 6321 location) (i) Critical shear stress at stud 1 (Node 7 location)

Fig. 10 Continued

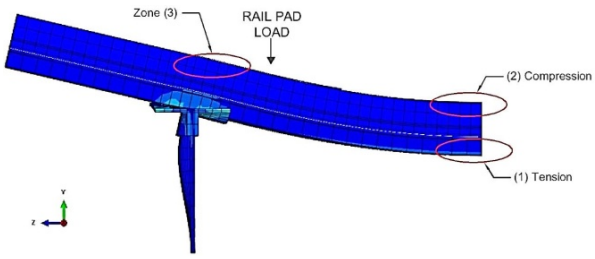

(a) Exaggerated deflected shape of the in-service panel at the full extent of loading

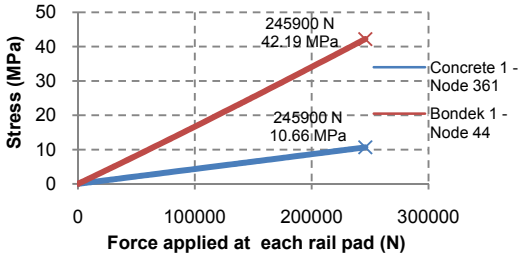

(b) Stress to load relationship for concrete and Bondek II nodes within zone (1) Tension

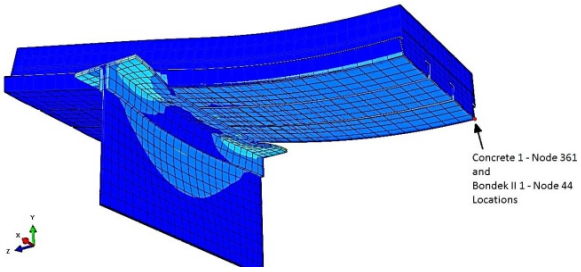

(c) Crucial zone of steel-concrete interface

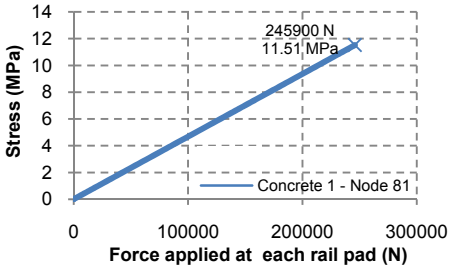

(d) Stress to load relationship for concrete node 81 within zone (2) Compression

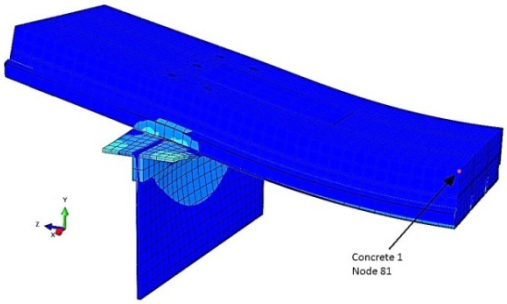

(e) Critical compression due to bending in concrete

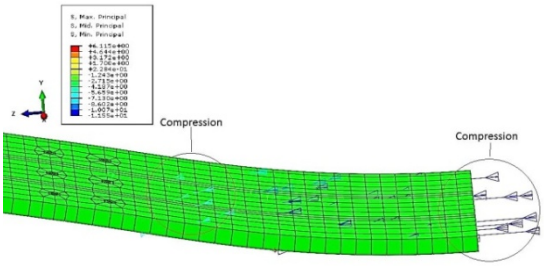

(f) Top concrete elements of the in-service panel subjected to compression only

Fig. 11 Finite element analysis of composite derailment panel – cont

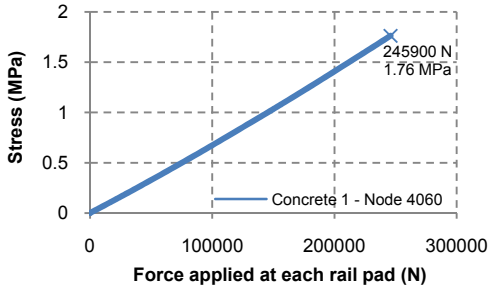

(g) Stress to load relationship for concrete node 4060 within zone (3) Compression

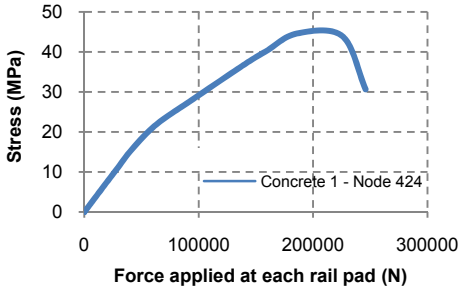

(h) Stress to load relationship for concrete node 424 acting in compression with the shear stud

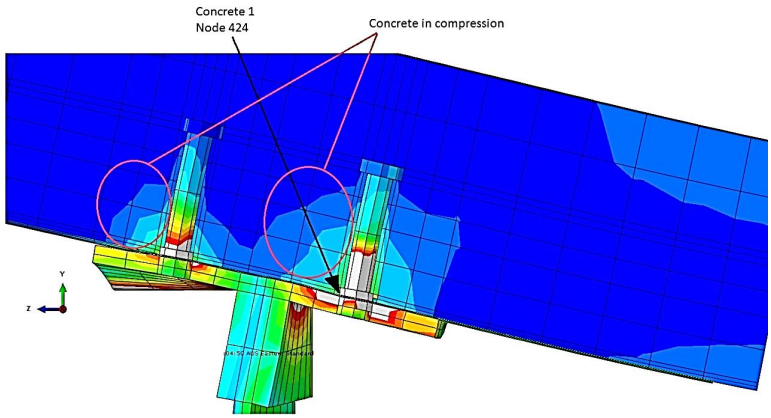

(i) Critical locations of concrete-stud interface

Fig. 11 Continued

derailment loads. This is less than the characteristic compressive stress of the concrete, which is 50 MPa, thus the concrete has not failed at ultimate loading.

The critical concrete node and the critical Bondek II node are shown in Figs. 10g and 10h respectively. The tensile stresses in both the concrete and the Bondek II increase linearly up to their maximum stresses of 14.28 MPa and 13.02 MPa respectively and correspond to the full magnitude of derailment loading. The tensile stress in the concrete at full loading exceeds the approximate cracking stress of 5.9 MPa as nominated in Section 6.3.2.2, however, the maximum stress within the Bondek II is significantly less than its yield strength of 550 MPa. This confirms the ample positive flexural capacity of the theoretically designed derailment panels. It can be noted that the stress in the base of the shear stud increases linearly up to a maximum stress of 251 MPa which is substantially less than the shear stud materials ultimate yield strength of 420 Mpa. The Bondek II has also not yielded upon application of the maximum derailment loads. Therefore, the shear studs and the steel shows promising capacity to withstand the maximum derailment loads, as shown in Fig. 10(i).

6.2 Performance of in-service panel

Fig. 11(a) indicates critical zones of the symmetrical half in-service panel subjected to ultimate in-service loads (excluding the derailment load combination). Fig. 11(b) shows the average stress

to in-service load relationship for the critical concrete and Bondek II nodes shown in Fig. 11(c). It can be noted from the graph that when the concrete starts to crack at low stress levels in the tension zone the Bondek II continues to sustain the tensile forces. The tensile stress present within the Bondek II at full application of the in-service loads is 42 MPa which is significantly less than the Bondek II yield stress of 550 MPa hence, mid span positive flexural strength is satisfied.

Fig. 11(d) illustrates average stress to in-service load relationship for the critical concrete node shown in Fig. 11(e) acting in compression. It can be noted that the stress increases at a constant rate up to a maximum compressive stress of 11 MPa at full application of the in-service loads. This is substantially less than the characteristic compressive stress of the concrete which is 50 MPa, thus the concrete has not failed under ultimate in-service loads. The theoretical designs for both the derailment and in-service panels considered a fully fixed connection at the shear stud locations. If a fully fixed connection is induced negative bending moments and hence tension in the top concrete fibres at the support is expected. This was the motive for designing conventional tensile reinforcing steel at the supports in the theoretical analysis. The ABAQUS models confirms that under an arbitrary serviceability load the assumption of fixed connections is appropriate, it was determined via the in-service models that under increased loads there is enough rotation at the shear stud locations to indicate a fully fixed condition dose not manifest. As a result, Fig. 11(f) shows the extreme top concrete fibres in zone 3 are only subjected to compressive forces and not tensile forces as was originally anticipated. Fig. 11(g) details the extent of the minor compressive stresses in the concrete at zone (3). It is also found that predominately compressive stresses occur in the conventional tensile reinforcing steel present at zone 3 while the minor tensile stresses shown are insignificant.

The tapering off of stress after reaching a maximum of approximately 45 MPa can be contributed to complex phenomenon of shear dowel strength as shown in Figs. 11(h) and (i). At a concrete stress of 45 MPa the young's modulus of the concrete is reduced and the load and hence stress is re-distributed to adjacent materials, in this case the shear studs. It can be noted that the stress in the base of the shear stud increases linearly up to a maximum of 243.9 MPa which is substantially less than the ultimate yield strength of 420 MPa. Therefore, the shear studs do not yield upon application of the maximum in-service loads. The stress in the Bondek II at the weld location around the base of the shear stud increases up to a maximum stress of 226 MPa, which is noticeably less than the Bondek II materials ultimate yield strength of 550 MPa.

7. Conclusions

Global demand of timber-replacement alternatives for railway construction and maintenance is significant, especially in some specific fit-for-purpose projects such as brown-field railway transom bridges. This paper presents a novel design of composite panels, which provide resiliency for either a spot replacement or a total renewal of aging timber components within railway infrastructure. Applications of composites to railway construction and maintenance require comprehensive considerations and systems thinking approach. This paper has demonstrates practical issues and systemic compliance requirements associated with the design of the composites.

Using the Sydney Harbour Bridge as a case study, the limitation of bearing capacity of existing bridge steel girders or stringers, low track clearances, insufficiency of spaces and cross sections of track structures due to existing overhead wiring structures, and so on, has proven that the designed

composite panels are a very attractive alternative. The composite panels have the capabilities of being precast and modulated in-order to reduce the depth, weight and required installation time relative to conventional slab track systems. Three dimensional finite element models of the composite panels have been developed to highlight critical design considerations and possible failure modes. This paper unlocks the design criteria for derailment loads, which previous research and most transom designs in practice have neglected to consider. Two innovative designs have been proposed: composite panels with or without derailment concern (so-called 'in-service' and 'derailment' panel, respectively). Comparing with traditional concrete direct-fixation slabs, the weight of the composite panels could be reduced by 20-24% and 10-12% for in-service and derailment panels, respectively. Taking into account constructability and maintainability, this paper is also aimed at providing a practical design and analysis guidance for railway engineers in order to safely and efficiently enable new composites as an essential part of railway infrastructure systems.

Acknowledgments

The authors are grateful to the Institute of Infrastructure Engineering, University of Western Sydney Australia for the financial support throughout this study. The second author wishes to thank Japan Society for the Promotion of Science for Invitation Research Fellowship (Long-term), Grant No. L15701, at Railway Technical Research Institute and the University of Tokyo, Japan. The authors are very grateful for the financial support from European Commission for H2020-MSCA-RISE Project No. 691135 "RISEN: Rail Infrastructure Systems Engineering Network," which enables a global research network that tackles the grand challenge in railway infrastructure resilience and advanced sensing under extreme conditions.

References

Atmaca, B. and Ates, S. (2012), "Construction stage analysis of three-dimensional cable-stayed bridges", *Steel Compos. Struct., Int. J.*, **12**(5), 413-426

Bonnett, C.F. (2005), *Practical Railway Engineering*, Imperial College Press, Hackensack, NJ, USA.

Bradford, M. and Uy, B. (2007), "Composite action of structural steel beams and precast concrete slabs for the flexural strength limit state", *Aust. J. Struct. Eng.*, **7**(2), 123-133.

Choi, J.Y., Park, Y.G., Choi, E.S. and Choi, J.H. (2010), "Applying precast slab panel track to replace timber track in an existing steel plate girder railway bridge", *Proc. Inst. Mech. Eng., Part F: J. Rail Rapid Transit*, **224**(3), 159-167.

Fanaie, N., Ghalamzan Esfahani, F. and Soroushnia, S. (2015), "Analytical study of composite beams with different arrangements of channel shear connectors", *Steel Compos. Struct., Int. J.*, **19**(2), 485-501.

Ferdous, W., Manalo, A., Van Erp, G., Aravinthan, T., Kaewunruen, S. and and Remennikov, A.M. (2015), "Composite railway sleepers–Recent developments, challenges and future prospects", *Compos. Struct.*, **134**(12), 158-168.

Goh, C.C., Patrick, M., Proe, D. and Wilkie, R. (1998), *Design of Composite Slabs for Strength - BHP Design Manual*, BHP Integrated Steel.

Griffin, D.W.P., Mirza, O., Kwok, K. and Kaewunruen, S. (2014), "Composites for railway construction and maintenance: A review", *The IES Journal Part A: Civil & Struct. Eng.*, **7**(4), 243-262.

Griffin, D.W.P., Mirza, O., Kwok, K. and Kaewunruen, S. (2015), "Finite element modelling of modular precast composites for railway track support structure: A battle to save Sydney Harbour Bridge", *Aust. J.*

Struct. Eng., **16**(2), 150-168.
Indraratna, B., Salim, W. and Rujikiatkamjorn, R. (2011), *Advanced Rail Geotechnology - Ballasted Track*, CRC Press, The Netherlands.
Kaewunruen, S. (2007), "Experimental and numerical studies for evaluating dynamic behaviour of prestressed concrete sleepers subject to severe impact loading", Ph.D. Thesis; School of Civil, Mining, and Environmental Engineering, University of Wollongong, Australia.
Kaewunruen, S. (2013), "Performance review of CarbonLoc material for alternative turnout bearers", Technical Report No. TR211; Track Services RailCorp, Australia, July, 17 p.
Kaewunruen, S. (2014), "Monitoring in-service performance of fibre-reinforced foamed urethane material as timber-replacement sleepers/bearers in railway urban turnout systems", *Struct. Monitor. Maint.*, **1**(1), 131-157. [Invited]
Kaewunruen, S. and Remennikov, A.M. (2007), "Field trials for dynamic characteristics of railway track and its components using impact excitation technique", *NDT & E. Int.*, **40**(7), 510-519.
Kaewunruen, S. and Remennikov, A.M. (2009a), "Progressive failure of prestressed concrete sleepers under multiple high-intensity impact loads", *Eng. Struct.*, **31**(10), 2460-2473.
Kaewunruen, S. and Remennikov, A.M. (2009b), "Structural safety of railway prestressed concrete sleepers", *Aust. J. Struct. Eng.*, **9**(2), 129-140. [Invited]
Kaewunruen, S., Remennikov, A.M. and Murray, M.H. (2011), "Greener & Leaner: Unleashing the capacity of railroad concrete ties", *ASCE J. Trans. Eng.*, **137**(4), 241-247.
Kaewunruen, S., Remennikov, A.M. and Murray, M.H. (2014), "Introducing limit states design concept to concrete sleepers: An Australian experience", *Frontiers in Mat.*, **1**(8), 1-3.
Kirkland, B. and Uy, B. (2015), "Behaviour and design of composite beams subjected to flexure and axial load", *Steel Compos. Struct., Int. J.*, **19**(3), 615-633.
Lam, D. and El-Lobody, E. (2001), "Finite element modelling of headed stud shear connectors in steel-concrete composite beam", (A. Zingoni Ed.), *Struct. Eng., Mech. Comp.*, Elsevier Science, Oxford, pp. 401-408.
Lezgy-Nazargah, M. and Kafi, L. (2015), "Analysis of composite steel-concrete beams using a refined high-order beam theory", *Steel Compos. Struct., Int. J.*, **18**(6), 1369-1389.
Li, F., Wu, P. and Liu, D. (2012), "Experimental study on the cable rigidness and static behaviors of AERORail structure", *Steel Compos. Struct., Int. J.*, **12**(5), 427-444.
Li, J., Huo, Q., Li, X., Kong, X. and Wu, W. (2014), "Dynamic stiffness analysis of steel-concrete composite beams", *Steel Compos. Struct., Int. J.*, **16**(6), 577-593.
Manalo, A., Aravinthan, T., Karunasena, W. and Ticoalu, A. (2010), "A review of alternative materials for replacing existing timber sleepers", *Compos. Struct.*, **92**(3), 603-611.
Mirza, O. and Uy, B. (2009), "Behaviour of headed stud shear connectors for composite steel-concrete beams at elevated temperatures", *J. Construct. Steel Res.*, **65**(3), 662-674.
Mirza, O. and Uy, B. (2011), "Behaviour of composite beam-column flush end-plate connections subjected to low-probability, high-consequence loading", *Eng. Struct.*, **33**(2), 647-662.
Mirza, O., Uy, B. and Patel, N. (2010), "Behaviour and strength of shear connectors utilising blind bolting", *Proceedings of the 4th International Conference on Steel and Composite Structures*, Sydney, Australia, July.
Mirza, O., Zhu, X. and Uy, B. (2011), "Condition assessment and strengthening of shear connection systems for composite bridges", *Sustainable Bridges*.
Domingo, L.M., Giner, B.B., Martín, C.Z. and Real Herraiz, J.I. (2014), "Experimental modal analysis of transverse-cracked RAILs- influence of the cracks on the real track behavior", *Struct. Eng. Mech., Int. J.*, **52**(5), 1019-1032.
Nguyen, H.T. and Kim, S.E. (2009), "Finite element modeling of push-out tests for large stud shear connectors", *J. Construct. Steel Res.*, **65**(10-11), 1909-1920.
Oehlers, D.J. and Bradford, M.A. (1995), *Composite Steel and Concrete Structural Members: Fundamental Behaviour*, Pergamon, New York, NY, USA.
Oehlers, D.J. and Bradford, M.A. (1999), "1 – Introduction", In: *Elementary Behaviour of Composite Steel*

and Concrete Structural Members, Butterworth-Heinemann, Oxford, UK, pp. 1-20.
Pecce, M., Rossi, F., Antonio Bibbo, F. and Ceroni, F. (2012), "Experimental behaviour of composite beams subjected to a hogging moment", *Steel Compos. Struct., Int. J.*, **12**(5), 395-412.
RailCorp (2010), *ESC 310 RailCorp Engineering Standard - Underbridges*.
RailCorp (2013a), *ESC 220 RailCorp Engineering Standard - Track Rail and Rail Joints*. URL: engineering.railcorp.nsw.gov.au/Disciplines/Civil/ESC_220.pdf
RailCorp (2013b), *ESC 230 RailCorp Engineering Standard - Sleepers and Track Support*. URL: engineering.railcorp.nsw.gov.au/Disciplines/Civil/ESC_230.pdf
Remennikov, A. and Kaewunruen, S. (2007), "Experimental determination of energy absorption capacity for railway prestressed concrete sleepers under impact loading", *Proceedings of the International Conference on Structural Engineering and Construction - ISEC2007*, Melbourne, Australia, September. [CD Rom]
Remennikov, A.M. and Kaewunruen, S. (2008), "A review of loading conditions for railway track structures due to train and track vertical interaction", *Struct. Cont. Health Monitor.*, **15**(2), 207-234.
Remennikov, A.M. and Kaewunruen, S. (2014), "Experimental load rating of aged railway concrete sleepers", *Eng. Struct.*, **76**(10), 147-162.
Remennikov, A.M., Murray, M.H. and Kaewunruen, S. (2011), "Reliability based conversion of a structural design code for prestressed concrete sleepers", *Proceedings of the Institute of Mechanical Engineering: Part F J. of Rail and Rapid Transit*, **226**(2), 155-173.
Standards Australia (2003a), Railway track material - Part 14: Prestressed concrete sleepers; *Australian Standard: AS1085.14-2003*.
Standards Australia, AS2327.1 2003 (2003b), "Composite structures - Simply supported beams", *Australian Standards*.
Standards Australia, AS5100.2 (2004), Bridge design - Part 2: Design loads, *Australian Standards*.
Standards Australia, AS3600 (2009), Concrete Structures, *Australian Standards*.
Shanmugam, N.E., Kumar, G. and Thevendran, V. (2002), "Finite element modelling of double skin composite slabs", *Finite Elem. Anal. Des.*, **38**(7), 579-599.
Shanmuganathan, S., Speers, R., Ruodong, P. and Sriskanthan, S. (2011), "Sydney Harbour Bridge: Replacement rail track support", *Proceedings of the 8th Conference on Austroads Bridge*, Sydney, Australia, October.
Tahmasebinia, F., Ranzi, G. and Zona, A. (2012), "A probabilistic three-dimensional finite element study on simply-supported composite floor beams", *Aust. J. Struct. Eng.*, **12**(3), 251-262.

DL

Nomenclature

A_p	Cross sectional area of the Bondek II
A_{pl}	Plan area
A_{sh}	Cross sectional area of the shear stud shank
A_{st}	Cross sectional area of tensile reinforcing steel
$A_{st,\min}$	Minimum required area of tensile reinforcing steel
b_h	Bedding thickness
b	Panel width
b_m	Total average rib width over a slab width of 1 m
b_v	Width of panel
C	Internal member compressive force
C_c	Internal compressive force in concrete
C_L	Lift coefficient
C_s	Internal compressive force in steel
D	Total panel depth
D_c	Overall depth of panel
$D_{\max,push}$	Ultimate strength of a shear connection
d	Effective depth to tensile reinforcing steel
d_{bs}	Shear connector shank diameter
d_0	Effective depth
d_p	Depth from the top of the panel to the centroid of the Bondek II
E_c	Young's modulus of concrete
E_s	Young's modulus of steel
f'_c	Characteristic compressive strength of concrete at 28 days
f'_{cj}	Characteristic cylinder strength of the concrete
$f_{ct,f}$	Concrete characteristic flexural tensile strength
f'_{cv}	Concrete shear strength
f_{sy}	Yield strength of tensile reinforcing steel
$f_{sy,f}$	Yield strength of shear reinforcement
$f_{sy,sh}$	Ultimate yield strength of the Bondek II
f_{uc}	Ultimate strength of shear stud material
$f_{vs,(AJAX)}$	Nominal shear strength of connections incorporating AJAX bolts
G_{panel}	Dead load of precast panels
H_r	Mechanical resistance between concrete and Bondek II

h_c	Concrete cover above profiled steel sheeting rib
h_r	Bondek II rib height
I_{cu}	Second moment of area for uncracked panel
I_p	Second moment of area of the profiled steel sheeting
K	Bondek II bending factor
k_b	Depth to centroid coefficient for balanced loading
k_u	Depth to centroid coefficient
L	Lever arm between internal compressive and tensile forces
M_u	Ultimate flexural capacity
$M_{u,sh}$	Nominal moment capacity of bare steel sheeting
P_{RD}	Nominal shear capacity of a headed shear stud
$Q_{breaking}$	Live loads from vehicle breaking
Q_{derail}	Live derailment loads
Q_{nosing}	Live nosing loads
Q_u	Ultimate strength shear stud connection
Q_{300LA}	Live load from 300LA vehicle loads
R^*	Reaction force
s	Shear fitment spacing
T	Internal member tensile force
T_{csc}	Resultant tensile force in Bondek II for complete shear connection
T_{sh}	Tensile force in Bondek II
$T_{y,sh}$	Tensile force within the Bondek II, per unit width
$T_{y,st}$	Tensile force within any conventional tensile reinforcement
t_{bm}	Base metal thickness of the Bondek II
V_{chem}	Shear strength due to chemical bond
V_{lock}	Shear strength due to interface interlock
V_s	Serviceability regional wind speed
V_u	Ultimate regional wind speed
V_{uc}	Shear capacity of concrete section
$V_{u,\min}$	Shear capacity of section incorporating minimum shear reinforcing
V_{us}	Shear capacity incorporating more than minimum reinforcing
W_{vs^*}	Service vertical wind load
W_{vu^*}	Ultimate vertical wind load
y_{sh}	Height at which T_{sh} acts above the soffit of the panel

z	Lever arm between internal compressive and tensile forces
$_{(+ve)}M^*$	Positive design moment
$_{(-ve)}M^*$	Negative design moment
$_{(+ve)}V^*$	Positive design shear force
$_{(-ve)}V^*$	Negative design shear force
ϕ	Reduction factor
H	Coefficient of friction
η	Modular ratio
ε_c	Strain in concrete
ε'_c	Strain in concrete at characteristic compressive stress
ε_{ps}	Plastic strain for steel
ε_{us}	Ultimate strain for steel
σ_c	Stress in concrete
σ_{us}	Ultimate steel stress
σ_{ys}	Yield steel stress
θ_v	Angle of shear cracking
N	Poisons ratio
ρ	Density